Super-Superexchange Influence on Magnetic Ordering in $Ni_3B_2O_6$ Kotoite

Svetlana N. Sofronova and Ilya I. Nazarenko*

Using ab initio software package WIEN2k, the calculations of electronic properties and of the energies of various magnetically ordered structures are carried out and possible mechanisms of magnetic ordering are analyzed in $Ni_3B_2O_6$. The superexchange (Ni-O-Ni) and super-superexchange interactions (Ni-O-B-O-Ni) are calculated, a magnetic ordering model is proposed.

1. Introduction

In recent years, much attention has been paid to compounds with geometric magnetic frustrations, since they have interesting magnetic properties and states spin glass, spin liquid, and spin ice.[1–4] A characteristic feature of these compounds is the presence of interconnected triangular or tetrahedral groups in the structure. Oxyborates $M_3B_2O_6$ (M = Co, Ni, or Mn) with a kotoite structure[5,6] contain structural elements that provide the prerequisites for the interesting magnetic properties: in their structure, there are triangular groups connected into ribbons. In the 1960s, kotoites with cobalt and nickel were synthesized. All three compounds are antiferromagnets, and although they are isostructural, their magnetic properties are different.[6] The first studies were carried out on powder samples. It was discovered that $Ni_3B_2O_6$ and $Co_3B_2O_6$ have one magnetic phase transition at 49 and 30 K, respectively, whereas $Mn_3B_2O_6$ is apparently characterized by two magnetic transitions at 55 and 35 K.[7] $Ni_3B_2O_6$ and $Co_3B_2O_6$ magnetic structures were studied in refs. [5,6]. It was found that their magnetic cell is four times larger than the crystallographic one. However, the authors were not completely convinced of their conclusions. An interesting feature of $Ni_3B_2O_6$ is the proximity of its paramagnetic Curie temperature (5 K) to zero, which may indicate competition between ferromagnetic and antiferromagnetic interactions, whereas the paramagnetic Curie temperature of $Co_3B_2O_6$ is quite typical for an antiferromagnet (63 K). Paramagnetic Curie temperature of $Mn_3B_2O_6$ exceeds the temperature of Neel six times, which may indicate the presence of strong frustrations in the system. However, the data given in refs. [5,6] are insufficient

to determine the magnetic structure of $Ni_3B_2O_6$ and the occurrence of magnetic order understanding in this compound.

In article,[8] the lattice dynamics was investigated by experimental and theoretical methods. Anomalous behavior of some Raman phonons was discovered in the region of the magnetic transition. The emergence of new phonon modes in the IR and Raman spectra at the magnetic transition temperature, according to the authors of ref. [8], indicate the existence of a new type magnetostructural phase transition in $Ni_3B_2O_6$. In a magnetically ordered state, ferromagnetically ordered chains are oriented antiferromagnetically relative to each other. The symmetry of the magnetic cell is P_a2_1/c, it is doubled relative to the primitive paramagnetic cell.

In this paper, we present the electronic and magnetic properties study of $Ni_3B_2O_6$ crystal. The calculations are performed in the framework of the density functional theory.[9,10] The exchange and correlation functional was processed by local spin density approximations (LSDA) and LSDA + U and the generalized Perdew–Burke–Ernzerhof gradient approximations GGA-PBE and GGA-PBE + U.

2. Crystal Structure

$Ni_3B_2O_6$ crystals belong to a space group *Pnnm* (kotoite structure).[6,11] The unit cell contains two formula units. Magnetic ions are Ni occupying two nonequivalent crystallographic positions 2a and 4f. Thus, in the unit cell, there are six magnetic ions. Nickel ions are located in oxygen octahedra, and boron ions are between oxygen octahedra. The structure of kotoite is illustrated in **Figure 1**. Bold lines denote chains of triangular groups in the *bc* plane. The structural feature of kotoite is the presence of ribbons extending along the *b* axis which are formed by triangular groups of Ni ions. If the exchange interactions are antiferromagnetic in triangular groups, then this can cause frustration.

3. Calculation Method

The electronic structure was calculated using the FP-LAPW + lo method.[12,13] The exchange-correlation energy was calculated using LSDA[14] and GGA-PBE[15] with additional Hubbard correlation coefficients describing the local electron–electron repulsion associated with Ni 3d-bands (LSDA + U and GGA-PBE + U).[16,17] The electron configuration of atoms used in our calculations was for Ni: [Ar] $3d^8$ $4s^2$, for B: [He] $2s^2$ $2p^1$, for O:

S. N. Sofronova, I. I. Nazarenko
Kirensky Institute of Physics of Federal Research Center KSC Siberian Branch Russian Academy of Sciences
Akademgorodok, 50, Building No. 38, 660036 Krasnoyarsk, Russia
E-mail: ilnz007@live.ru

The ORCID identification number(s) for the author(s) of this article can be found under https://doi.org/10.1002/pssb.201900060.
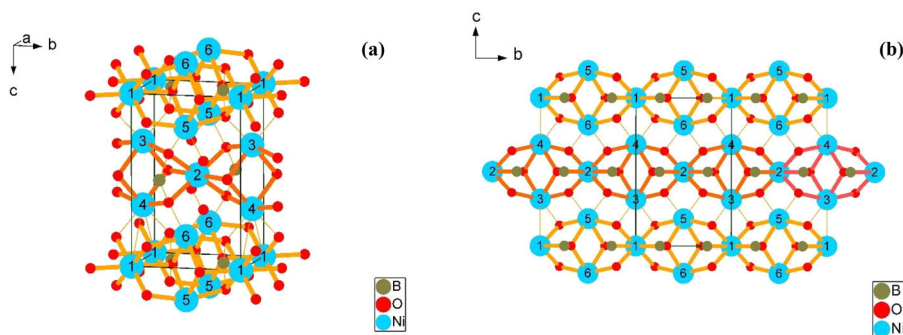
Figure 1. The unit cell of kotoite structure: (a) perspective view, (b) bc-plane view. Bold lines show triangular groups in the bc plane. Ions 1, 2 belong to crystallographic position 2a, ions 3–6 belong to position 4f.
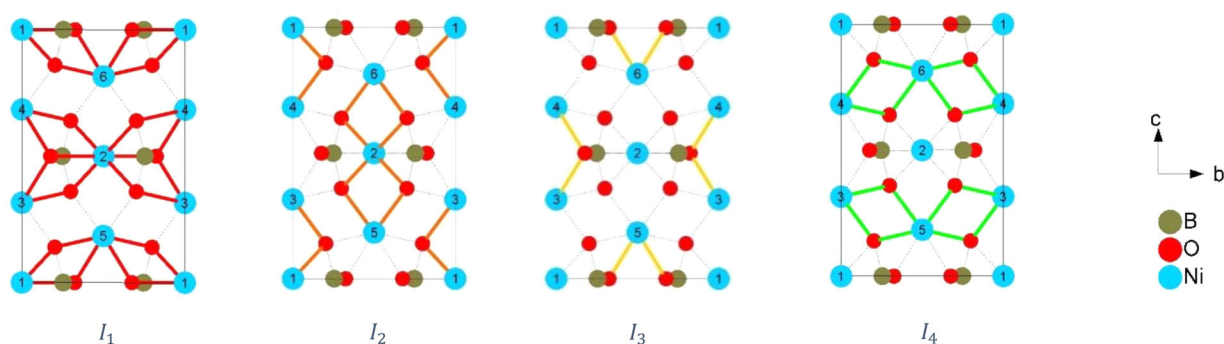
Figure 2. Different types of exchange interactions in the kotoite unit cell used to calculate the model.

[He] $2s^2 2p^4$. All calculations were carried out using experimental lattice parameters and atomic coordinates. The minimization of the lattice parameters gave values very close to the experimental ones from ref. [6] (the difference is less than 1%), the minimization of the internal parameters was not carried out because of their large number. Total energy was minimized using a set of 400 k-point in the complete Brillouin zone of the unit cell ($a = 4.529\,\text{Å}$, $b = 5.462\,\text{Å}$, and $c = 8.436\,\text{Å}$), value 7.0 for $R_{mt}K_{max}$ was used for all studied configurations. Self-consistent calculations converge to $1\,\mu\text{Ry}$. The radii of the MT-spheres are 2.02 atomic units for Ni, 1.30 a.u. for B and O. The total density of states (DOS) was obtained using the modified tetrahedra

Table 1. Energies of magnetic structures with expressions and spin configurations.

Conf.	Ni_1	Ni_2	Ni_3	Ni_4	Ni_5	Ni_6	Energy expression	E (Ry)	ΔE (10^{-5} Ry) set A	ΔE (10^{-5} Ry) set B
a	↑	↑	↓	↓	↓	↓	$8I_1 + 8I_2 - 8I_4 - 2I_3 - e_0$	−20232.282558	−2.7	−3.8
b	↓	↑	↓	↓	↑	↑	$8I_1 - 8I_2 + 8I_4 - 2I_3 - e_0$	−20232.282290	3.5	0
c	↓	↓	↓	↑	↑	↑	$-4I_1 - 4I_2 - e_0$	−20232.283478	0	0
d	↓	↑	↓	↓	↓	↑	$-4I_1 + 4I_2 - e_0$	−20232.283454	0	−1.8
e	↓	↑	↓	↑	↓	↓	$4I_1 - 4I_2 - e_0$	−20232.283846	0	−1.6
f	↓	↓	↓	↓	↓	↑	$4I_1 + 4I_2 - e_0$	−20232.283874	5.2	1.9
g	↓	↑	↑	↑	↓	↓	$-8I_1 + 8I_2 + 8I_4 - 2I_3 - e_0$	−20232.283070	3.1	0
h	↑	↑	↑	↑	↑	↑	$-8I_1 - 8I_2 - 8I_4 - 4I_3 - e_0$	−20232.283350	7.7	0
i	↓	↑	↑	↓	↓	↑	$-2I_2 - 8I_4 - e_0$	−20232.284331	−4.0	−2.9
j	↓	↑	↓	↑	↓	↑	$2I_2 - 8I_4 - e_0$	−20232.284653	0	0
k	↓	↓	↓	↓	↑	↑	$-2I_2 + 8I_4 - e_0$	−20232.282705	5.8	2.5
l	↑	↓	↑	↑	↑	↑	$-2I_2 - 8I_4 - e_0$	−20232.282929	0	−4.4

Table 2. Comparison of the indirect exchange interactions values obtained using different sets of full energies of $Ni_3B_2O_6$.

Spin configuration set	I_1 (K)	I_2 (K)	I_3 (K)	I_4 (K)	e_0 (Ry)
Set A conf. c, d, e, j, l	3.6	−0.2	−34.0	1.4	−20232.283650
Set B conf. b, c, g, h, j	3.8	−0.1	−33.2	1.4	−20232.283667
Work[7]	6.2	2.8	6.2	−6.2	–

Table 3. Evaluation of energies from exchange interaction constants from ref. [7].

Conf.	E (K) from constants of ref. [7]	E (K) from constants of set A	E (K) from constants of set B
a	218.4	168.2	169.0
b	−69.6	220.3	217.3
c	72.0	27.2	29.8
d	27.2	30.9	30.8
e	−27.2	−30.9	−30.8
f	−72.0	−27.2	−29.8
g	−178.4	96.5	94.2
h	−69.6	59.5	50.0
i	−74.4	−113.8	−109.5
j	124.0	−158.4	−155.8
k	−124.0	158.4	155.8
l	74.4	113.8	109.5

method of Blöchl et al.[18] We used $U = 0.52$ Ry and $J = 0$ Ry in the LSDA + U and GGA-PBE + U schemes.

4. Results and Discussion

4.1. Magnetic Structure

To analyze magnetic ordering, it is necessary to determine the super-exchange interactions between nickel ions Ni-O-Ni. In the structure of kotoite, there are four types of super-exchange interactions between pairs of magnetic ions i and j, I_n where $n = 1 \div 4$ (**Figure 2**).

To determine the magnitude of the exchange interactions, 12 spin configurations were chosen that determine the magnetic structure (**Table 1**) in the crystallographic unit cell. Six of them are ferrimagnetic: a, d, e, f, k, l, five are antiferromagnetic: b, c, g, i, j, and one is ferromagnetic – h. General view of the total energy expression is

$$E_m = -\left(\frac{1}{2} \sum_{ij} J_{ij} \langle s_i \cdot s_j \rangle + e_0 \right) \tag{1}$$

where $J_{15}, J_{16}, J_{23}, J_{24}, J_{32}, J_{42}, J_{51}, J_{61}$ – exchanges of I_1 type, $J_{13}, J_{14}, J_{25}, J_{26}, J_{31}, J_{41}, J_{52}, J_{26}$ – exchanges of I_2 type, $J_{34}, J_{56}, J_{43}, J_{65}$ – exchanges of I_3 type, $J_{35}, J_{46}, J_{42}, J_{53}, J_{64}$ – exchanges of I_4 type, the rest types $J_{ij} = 0$.

Since the number of spin configurations for the determination of the constants is redundant, we can choose different sets of configurations to determine I_n. Calculated I_n values for different sets of spin configurations are given in **Table 2**, as well as I_n values defined in ref. [7] using semi-empirical method.[19–22] The difference between the energies calculated from a set of spin configurations A and B using formula (1) is given in Table 1. As can be seen from Table 2, the exchange interactions for different sets of spin configurations are very close. Set B gives the smallest divergence of energy E_m values (Table 1).

The strongest super-exchange interaction is I_3. This interaction is inside the ribbons. In contrast to the semi-empirical calculation, this exchange interaction is antiferromagnetic. Another exchange, inside the triangular ribbons, I_1, is ferromagnetic, and it is of a smaller magnitude order. Inter-ribbon exchanges I_2 and I_4 are weak, I_2 exchange is almost zero.

When the magnetic cell coincides with the crystallographic one, the most energetically favorable magnetic structures for the case are depicted in **Figure 3**. It should be noted that both of these structures are antiferromagnetic, which is consistent with experimental data. In both cases, the system contains frustrating
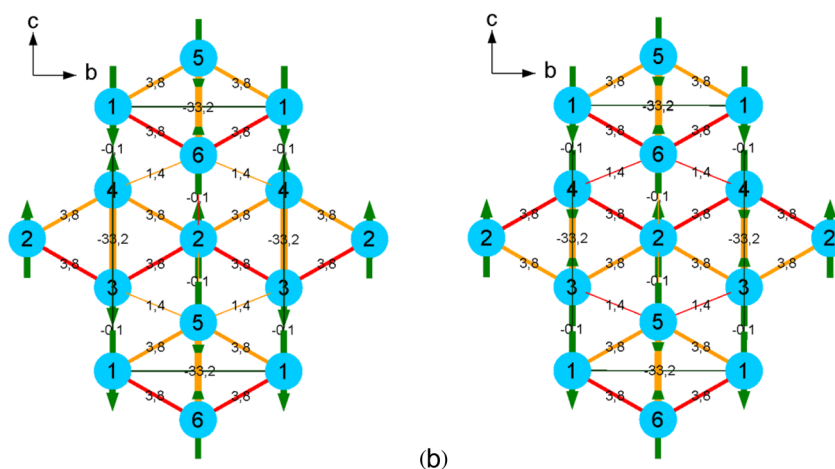
Figure 3. Possible magnetic structures for the spin configurations j (a) and i (b), frustrated exchange interactions are highlighted in red.

interactions (marked in red in the figure). Calculation using exchange interactions obtained from semi-empirical calculations[7] gives a ferrimagnetic structure as the most advantageous (**Table 3**). However, according to experimental data,[5] the $Ni_3B_2O_6$ magnetic cell is four times bigger than the
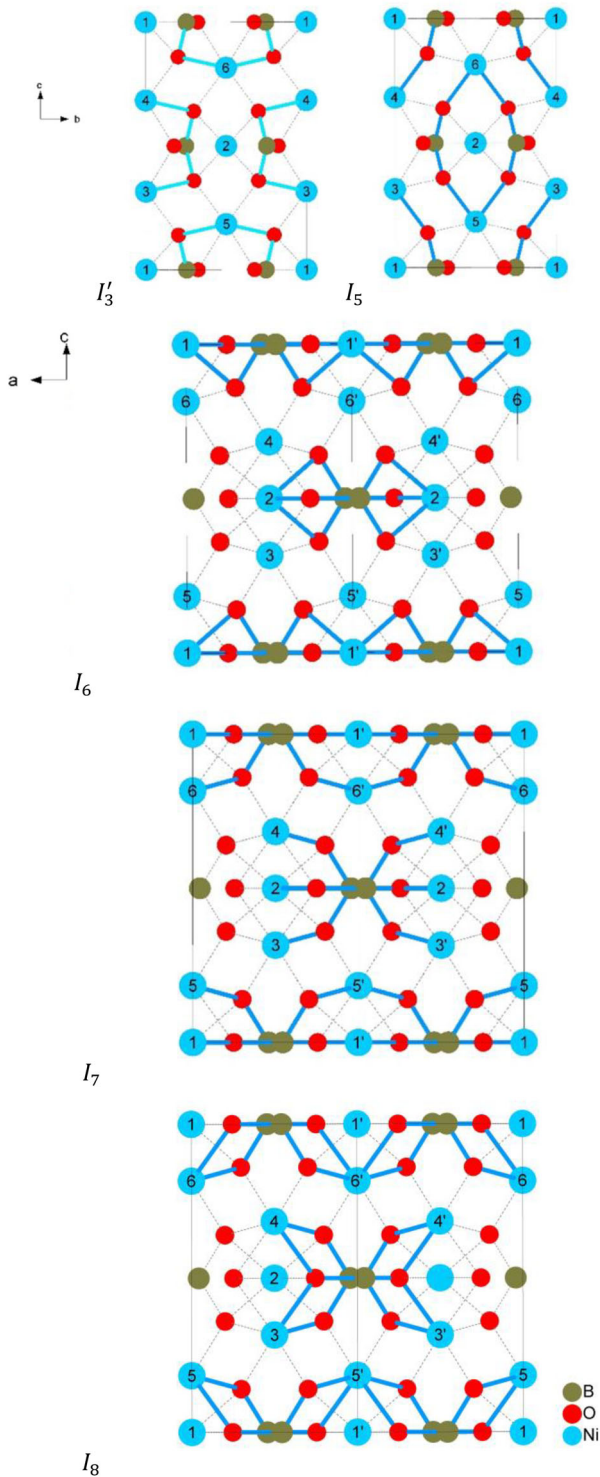
Figure 4. Paths of super-superexchanges Ni-O-B-O-Ni in $Ni_3B_2O_6$.

Table 4. Energies and their expressions in terms of exchange interaction constants for a crystallographic cell doubled along the a- and c-axis.

Conf.	1	1'	2	2'	3	3'	4	4'	5	5'	6	6'	Energy expression	E (Ry)
2a														
a	←	→	←	→	←	→	→	←	←	→	→	←	$-4I_3 - 4I_5 - 8I_6 - 4I_8 - e_0$	−40464.568841
b	←	←	←	→	←	←	→	→	←	→	→	←	$-4I_3 - 4I_5 - e_0$	−40464.568893
c	→	←	→	←	→	←	←	←	→	→	←	→	$4I_3 + 4I_5 - 8I_6 - 4I_8 - e_0$	−40464.566960
d	←	→	←	→	←	→	←	→	→	←	→	→	$4I_3 + 4I_5 - 8I_7 - e_0$	−40464.566774
e	→	←	→	←	←	←	←	←	→	→	→	←	$-8I_6 - e_0$	−40464.567802
2c														
a	→	→	←	←	←	←	→	→	←	→	←	→	$-4I_3 - e_0$	−40464.568336
b	←	←	→	→	→	→	→	→	←	→	←	→	$4I_3 - e_0$	−40464.568334
c	→	←	←	←	←	←	←	←	→	→	→	→	$-4I_5 - e_0$	−40464.568162
d	→	→	←	←	←	←	←	←	→	→	←	←	$4I_5 - e_0$	−40464.568334

Table 5. Calculated constants values $I_3 + I_3'$, I_5, I_6, I_7, I_8.

I_n	$I_3 + I_3'$	I_5	I_6	I_7	I_8
I_n (K)	−0.11	2.45	−2.14	−3.48	2.80

Table 6. Recalculated values of exchange interactions taking into account the contributions of super-superexchange interactions to energy.

	I_1	I_2	I_3	I_4	I_5	I_6	I_7	I_8
I_n (K)	2.67	−6.36	−0.11	8.36	2.45	−2.14	−3.48	2.80

Table 7. Energy values depending on the direction of the magnetic moment in the crystal.

Direction	$E_{[uvw]}$ (Ry)
[100]	−20233.388584
[010]	−20233.388584
[001]	−20233.388676

crystallographic one. Based on the magnitudes and signs of the super-exchange interactions obtained in this paper, it is difficult to understand the reasons for the magnetic cell growth, relative to crystallographic one.

Super-exchange interaction I_3' (**Figure 4**) impossible to split with superexchange interaction I_3. In order to highlight the exchange interaction I_5, it is necessary to increase the unit cell along the c-axis. For calculating exchange interactions I_6, I_7, I_8, it is needed to increase the unit cell along a. In order to highlight I_4', it is necessary to increase the unit cell eight times. However, at the moment our computational resources do not allow the calculation of even a cell that is four times larger than a unit cell. In this regard, we were able to determine the super-super-exchange interactions I_5, I_6, I_7, I_8 (Figure 4).

In **Table 4**, there are energies expressions for cells doubled along the c- and a-axes.

Using the results of energy calculations for double-cell magnetic structures (**Table 5**), we defined constants I_5, I_6, I_7, I_8 and recalculated constant $I_3 \equiv (I_3 + I_3')$ (Table 5).

As can be seen from Table 5, the calculated values of super-superexchange interactions are comparable in magnitude with the super-exchange interactions. In addition, the exchange interaction I_3 is almost zero. Antiferromagnetic exchange

interactions I_6, I_7 bind adjacent ribbons of triangular groups. An increase of the magnetic cell with respect to the crystallographic one can be associated with these interactions.

Since in the case when the magnetic cell coincides with crystallographic one, super-superexchange interactions cannot be split from the superexchange interactions, we recalculated the interactions I_1, I_2, I_4 considering the contributions to the energy of super-superexchange interactions. The results are shown in **Table 6**.

As can be seen from Table 6, after recalculating the interaction inside the ribbon, either ferromagnetic (I_1), or very weak (I_3).

And it can be expected that the ordering in the ribbons is ferromagnetic. The exchange interactions between the ribbons are the strongest, and they compete with each other, such competition can lead to zero Curie-Weiss temperature.

Both superexchange interaction I_2 and super-superexchange interactions I_6, I_7 are antiferromagnetic, and it is possible that an increasing of the magnetic cell relative to the crystallographic one is associated with them.

The orientation of the magnetic moments on the ions was not estimated in ref. [5], but a rhombic magnetic cell ($2a \times b \times 2c$) was proposed. In ref. [8], there was also a magnetic cell – a monoclinic one with doubling of the primitive cell relative to the paramagnetic phase ($2a$, $-b$, $a+c$, 0.0.0). In both papers, it is mentioned that the ribbons are ferromagnetically ordered. In **Figure 5**, we presented three magnetic structures in which neighboring ribbons are oriented in different ways relative to each other. In Figure 5c, a magnetic cell can be selected in a rhombic structure and then it will be a quadruple cell $2a \times b \times 2c$
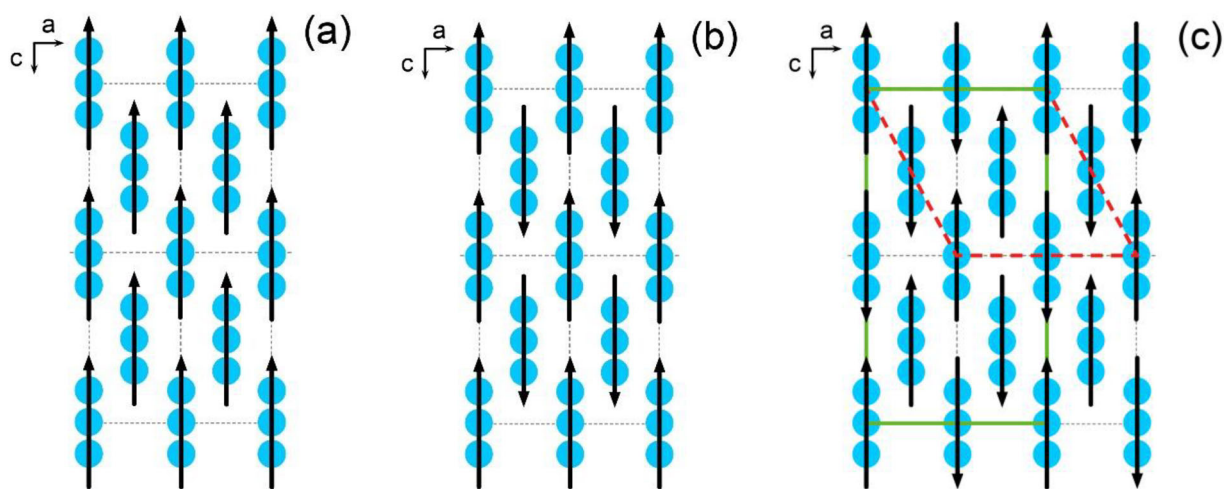
Figure 5. Different types of magnetic ordering during ferromagnetic ordering inside triangular ribbons.
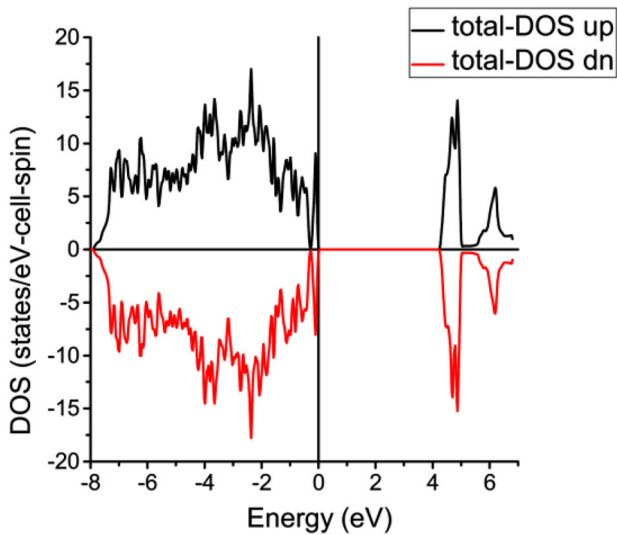
Figure 6. Graph of the total density of states of the $Ni_3B_2O_6$ antiferromagnetic structure. The Fermi level is at 0 eV.

relative to the paramagnetic phase (solid circuit in Figure 5c) or in a monoclinic structure and then this cell will be doubled relative to the paramagnetic phase (dotted outline on Figure 5c).

We calculated the energies of these three types of magnetic ordering using a double monoclinic cell, the most favorable type of magnetic ordering is shown in Figure 5c, the magnetic structure shown in Figure 5b is the least advantageous. If we take

as 0 the energy of the ferromagnetic magnetic structure (Figure 5a), then the difference in energy from the magnetic structures shown in Figure 5b will be $+5.5 \cdot 10^{-4}$ Ry, and with the structure shown in Figure 5c $-8.5 \cdot 10^{-5}$ Ry. If we estimate the energies of these magnetic structures using only the resulting Ni-O-Ni exchange interactions, the ferromagnetic structure will be most beneficial, but if we take into account all types of exchange interactions, including the super-superexchange Ni-O-B-O-Ni interactions, then the most favorable is the ordering shown in Figure 5c, which is consistent with the magnetic ordering found in refs. [5,8].

We also tried to determine the most favorable orientation of the magnetic moments with respect to crystallographic directions. According to experimental data, the magnetic moments in $Ni_3B_2O_6$ are directed along the c-axis. We calculated the energies for the ferromagnetic state taking into account spin–orbit interactions, when the direction of the magnetic moments coincides with the crystallographic directions (**Table 7**). As seen from Table 7, orientation of magnetic moments along the c-axis is also profitable.

4.2. Electronic Structure

In **Figure 6**, the total density of states is presented for the most favorable magnetic structure j. As can be seen from Figure 6, $Ni_3B_2O_6$ is a dielectric with a band gap of 4.08 eV.

In **Figure 7**, partial densities of states of Ni's 3d and O's 2p electrons are presented. As can be seen from the graphs, the
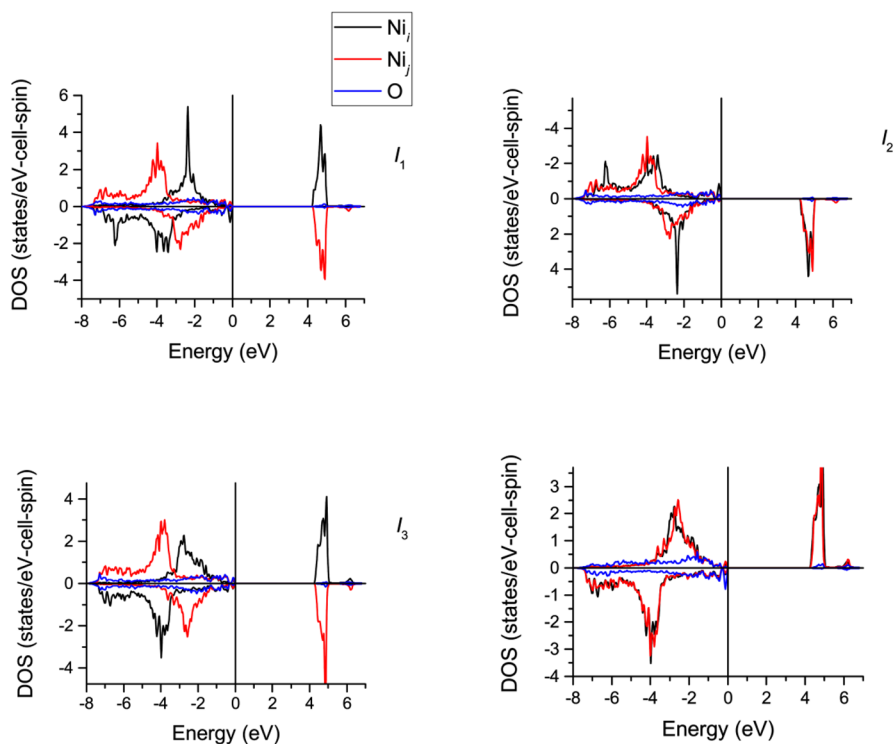
Figure 7. Partial density of states for 3d Ni and 2p, located between interacting nickel atoms for exchange interactions I_1, I_2, I_3, and I_4. Negative densities are indicated for spin-down states. The Fermi level is at 0 eV.

Table 8. Local magnetic moments of atoms in the unit cell of $Ni_3B_2O_6$.

Position	2a		4f	4g	8h	
Atom	Ni_1, Ni_2	Ni_3, Ni_6	Ni_4, Ni_5	O_1, O_2, O_3, O_4	O_5, O_8, O_{10}, O_{11}	O_6, O_7, O_9, O_{12}
Moment, μ_B	1.766	1.801	1.798	0.024	0.07	0.006

valence band and the conduction band do not intersect (which is typical for insulators), and the density of states has a zero value (of charge carriers) at the Fermi level. From this, we can assume that direct and RKKY-exchange interaction will not be effective in $Ni_3B_2O_6$. To describe the mechanisms of magnetic transition in $Ni_3B_2O_6$, it is worth to refer to the mechanism of indirect exchange interaction (super-exchange).

The magnetic moments of metal ions in a crystallographic cell were also determined (**Table 8**). Nickel magnetic moment is close to nominal, equal to $2\,\mu_B$. Oxygen ions also have a weak magnetic moment due to hybridization with nickel atoms (Figure 7).

5. Conclusion

In this paper, we attempted to analyze the magnetic ordering in a low-dimensional kotoite using the Wien2k software package. Calculations of the band structure showed that the material is an insulator, and direct exchange interaction in the connection are not effective.

The calculated magnetic moments are close to the nominal value $2\,\mu_B$.

Taking into account the spin–orbit interaction gives the most favorable orientation along the *c*-axis that is consistent with experimental data.

Using the energies of various magnetically ordered states, we estimated the magnitudes of indirect superexchange (Ni-O-Ni) and super-superexchange interactions (Ni-O-B-O-Ni). The magnitudes of superexchange and super-superexchange interactions are of the same order and there is a competition between ferromagnetic and antiferromagnetic exchange interactions. The contribution of superexchange (Ni-O-Ni) and super-superexchange interactions (Ni-O-B-O-Ni) is important in the formation of magnetic order. It is likely that the antiferromagnetic super-superexchange interactions Ni-O-B-O-Ni are responsible for the increase in the magnetic cell relative to the crystallographic one. Magnetic structure with a cell $2a \times b \times 2c$ has the lowest energy. It is the same as defined in $Co_3B_2O_6$ using neutron scattering.[5] In experimental work for $Ni_3B_2O_6$, the directions of the magnetic moments on the ions have not been established.

Conflict of Interest

The authors declare no conflict of interest.

[1] Z. He, T. Kyômen, T. Taniyama, M. Itoh, *J. Solid State Chem.* **2006**, *179*, 3937.
[2] W. Miiller, M. Christensen, A. Khan, N. Sharma, R. Macquart, M. Avdeev, G. McIntyre, R. Piltz, C. Ling, *Chem. Mater.* **2011**, *23*, 1315.
[3] R. Goff, A. Williams, P. Attfield, *Phys. Rev. B* **2004**, *70*, 014426.
[4] K. Hayashi, T. Nozaki, R. Fukatsu, Y. Miyazaki, T. Kajitani, *Phys. Rev. B* **2009**, *80*, 144413.
[5] R. Newnham, M. Redman, R. Santoro, *Z. Kristallogr.* **1965**, *121*, 418.
[6] R. Newnham, R. Santoro, P. Seal, G. Stallings, *Phys. Status Solidi B* **1966**, *16*, K17.
[7] L. N. Bezmaternykh, S. N. Sofronova, N. V. Volkov, E. V. Eremin, O. A. Bayukov, I. I. Nazarenko, D. A. Velikanov, *Phys. Status Solidi B* **2012**, *249*, 1628.
[8] R. V. Pisarev, M. A. Prosnikov, V. Y. Davydov, A. N. Smirnov, E. M. Roginskii, K. N. Boldyrev, A. D. Molchanova, M. N. Popova, M. B. Smirnov, V. Y. Kazimirov, *Phys. Rev. B* **2016**, *93*, 134306.
[9] W. Kohn, L. J. Sham, *Phys. Rev.* **1965**, *140*, A1133.
[10] P. Hohenberg, W. Kohn, *Phys. Rev.* **1964**, *64*, B864.
[11] J. Pardo, M. Martinez-Ripoll, S. García-Blanco, *Acta Crystallogr. Section B* **1974**, *30*, 37.
[12] P. Blaha, K. Schwarz, G. Madsen, D. Kvasnicka, J. Luitz, *An Augmented Plane Wave + Local Orbitals Program for Calculating Crystal Properties*. Vienna University of Technology Inst. of Physical and Theoretical Chemistry, Vienna **2015**.
[13] E. Sjöstedta, L. Nordströma, D. Singhb, *Solid State Commun.* **2000**, *114*, 15.
[14] J. Perdew, Y. Wang, *Phys. Rev. B* **1992**, *45*, 13244.
[15] J. P. Perdew, K. Burke, M. Ernzerhof, *Phys. Rev. Lett.* **1996**, *77*, 3865.
[16] V. I. Anisimov, J. Zaanen, O. K. Andersen, *Phys. Rev. B* **1991**, *44*, 943.
[17] V. I. Anisimov, I. V. Solovyev, M. A. Korotin, M. T. Czyżyk, G. A. Sawatzky, *Phys. Rev. B* **1993**, *48*, 16929.
[18] P. E. Blöchl, O. Jepsen, O. K. Andersen, *Phys. Rev. B* **1994**, *49*, 16223.
[19] O. A. Bayukov, A. F. Savitskii, *Phys. Status Solidi B* **1989**, *155*, 249.
[20] O. A. Bayukov, A. F. Savitskii, *Fizika Tverdogo Tela* **1994**, *36*, 1923.
[21] P. W. Anderson, *Phys. Rev.* **1959**, *115*, 2.
[22] M. V. Eremin, *Fizika Tverdogo Tela* **1982**, *24*, 423.